Journal of the Physical Society of Japan **83**, 014713 (2014)
http://dx.doi.org/10.7566/JPSJ.83.014713

Intermolecular THz vibrations relevant to optically and thermally induced magnetic phase transitions in the strongly correlated organic radical TTTA

Taro Kawano[a)], Ikufumi Katayama[a)], Jun Ohara[a),*], Masaaki Ashida[b)], and Jun Takeda[a)]

[a)] *Department of Physics, Graduate School of Engineering, Yokohama National University Yokohama 240-8501, Japan*

[b)] *Graduate School of Engineering Science, Osaka University, Toyonaka 560-8531, Japan*

(Received August 16, 2013; accepted November 20, 2013; published online December 24, 2013)

Intermolecular vibrations relevant to optically and thermally induced magnetic phase transitions between low temperature (LT) diamagnetic and high temperature (HT) paramagnetic phases in a strongly correlated organic radical 1,3,5-trithia-2,4,6-triazapentalenyl (TTTA) crystal have been investigated using broadband terahertz (THz) time-domain spectroscopy. Two absorption bands with different polarizations were clearly observed at 1.3 and 4.0 THz in the LT phase, whilst absent in the HT phase. The temperature dependence of the THz absorption peak exhibits hysteretic behavior around room temperature, indicating that the observed THz absorption bands are related to the magnetic phase transition in TTTA. Considering the symmetry of the crystal using group theoretical analysis, the observed absorption bands are attributed to intermolecular vibrations with A_u symmetry. We found that the absorption band at 4.0 THz disappeared upon irradiation by a laser pulse with a photon density greater than 3.0×10^{18} photons/cm^2. These results show that probing the intermolecular THz vibrations is indispensable for revealing the photoinduced phase transition from the LT diamagnetic to HT paramagnetic phase.

*Current address: Department of Physics, Hokkaido University, Sapporo 060-0810, Japan.

I. Introduction

The photoinduced phase transition (PIPT) and its related macroscopic properties have attracted much interest with regards to both fundamental physics research and the potential for future applications, such as optical switching devices. This is because the PIPT involves nonlinear and non-equilibrium processes resulting from cooperative interactions between excited states.[1-8] According to the theoretical framework for PIPT dynamics, the cooperative interactions induced by photoexcitation stimulate the formation of a domain accompanied by local lattice distortions; a precursor of the PIPT. The domain subsequently multiplies in size by an avalanche effect, leading to a macroscopic phase transition.[1-3] Ultrafast measurements are therefore indispensable when it comes to understanding the whole PIPT mechanism by revealing the electron-phonon dynamics, and have been extensively applied to various kinds of materials showing PIPTs, for example organic ionic crystals.[9-13] By performing ultrafast pump-probe spectroscopy, the low frequency lattice vibrations related to the PIPT—which are assigned as Raman active modes—generally manifest as oscillatory components in the reflectivity and absorbance change spectra. In contrast to the Raman active modes, little is known about the complementary infrared (IR) active modes that are also relevant to the PIPT. The recent development of terahertz time-domain spectroscopy (THz-TDS) has enabled the investigation of IR active modes.[14-17]

The strongly correlated organic radical, 1,3,5-trithia-2,4,6-triazapentalenyl (TTTA), is a promising candidate for the study of PIPT dynamics. TTTA has a very simple molecular structure consisting of only eight atoms: three sulfur, three nitrogen, and two carbon atoms. Its crystal exhibits a metastable magnetic state around room temperature (RT), as evidenced by the significant hysteresis between the low temperature (LT) diamagnetic phase and the high temperature (HT) paramagnetic phase.[18,19] Owing to the simple molecular structure and interesting magnetic properties, the electronic density of states of the TTTA crystal has also been modeled. It was found that the HT phase is a Mott insulator consisting of a one-dimensional stack of evenly spaced molecules due to strong correlation between unpaired electrons in the TTTA molecules, whilst the LT phase is a Peierls insulator that forms dimers.[2,20,21] Therefore, probing the intermolecular vibrations between TTTA molecules relevant to the stacking direction is straightforward and crucial for revealing the PIPT mechanism.[20] The properties of the PIPT were previously studied by photoinduced electron spin resonance (ESR) and

Raman scattering.[22-24] Recently, the dynamics of the conversion from the self-trapped exciton (STE) state with local lattice distortions to the macroscopic photoinduced HT phase was investigated by photoluminescence (PL) and Raman scattering.[25-27] Under the two-photon absorption for the charge transfer (CT) exciton band, the PIPT from the LT to the HT phase via the STE state could be achieved. The PL due to the STE state in the LT phase first showed a red-shift and a decrease in the intensity with increasing photon density, finally reaching a critical photon density of 3.0×10^{18} photons/cm^2, after which the PIPT occurs. Subsequently, the Raman intensity in the HT phase increases with a slightly higher threshold photon density of 6.0×10^{18} photons/cm^2.[27] These experiments show that the STE really acts as a trigger for the PIPT, and that the PIPT from the LT to HT phase eventually completes via the STE states. However, the observed photoinduced Raman modes in the HT phase are located in the frequency region of 150-3000 cm^{-1} and are thereby assigned to the intramolecular vibrations of the TTTA molecule. The low frequency intermolecular vibrations that directly influence the PIPT through dimerization of the TTTA molecules, on the other hand, are still not well understood.

In the present work, we investigate intermolecular vibrations in TTTA single crystals using broadband THz-TDS. We identified two THz absorption bands in the LT phase at 1.3 and 4.0 THz that are not present in the HT phase; the two absorption bands had different polarizations. The IR active and inactive intermolecular vibrations in the LT and HT phases, respectively, are then revealed by group theory. The absorption band at 4.0 THz disappears above a threshold photoexcitation, indicating that the PIPT from the diamagnetic LT state to the paramagnetic HT state takes place. These results demonstrate that broadband THz-TDS is a powerful spectroscopic tool in the search for intermolecular vibrational modes relevant to the PIPT.

II. Experimental

The TTTA crystals discussed here were grown by the sublimation technique, further details of which were reported elsewhere.[23,28] As-grown crystals were prepared in the HT state with typical dimensions of 1.0 x 0.5 x 0.1 mm^3. In order to measure the polarized transmittance spectra in the THz frequency region, as-grown TTTA crystals with a thickness of less than 0.1 mm were chosen. Two of these HT phase crystals were mounted onto two of four holes located on a copper plate sample holder with the *b*-axis

aligned either longitudinally or vertically with respect to the horizontal direction of the sample holder, as shown in Fig. 1(a). The other two holes were used to measure polarized reference THz waves. Since TTTA crystals are volatile, the sample holder was sandwiched by two additional thin copper plates and sealed with Si windows. LT phase crystals were obtained by cooling the HT phase crystals for several hours in a temperature-controlled cryostat at liquid nitrogen temperature.

Figure 1(b) shows the experimental setup for our broadband THz-TDS. In our measurements we used a mode-locked Ti:sapphire laser as the light source, with a pulse duration of 20 fs; repetition rate of 78 MHz; central wavelength of 800 nm; and an average power of 400 mW. The laser output was divided into two beams: one main part was used as a pump pulse to generate a THz wave that was focused onto a photoconductive antenna with a 400 μm gap; the other beam was used as a probe pulse and was focused onto a dipole-type photoconductive antenna (GaAs) with a 5 μm gap in order to detect the THz wave. A bias voltage of 250 V was applied to the generation antenna to enhance the intensity of the terahertz wave and the optical setup was purged with nitrogen gas to reduce water vapor. To avoid phonon absorption by the GaAs antennas, both the generation and detection antennas were used in the reflective configuration. Further details of this experiment are reported elsewhere.[29,30)]

When performing photoconversion from the LT to HT phase, we used an optical parametric oscillator (OPO) coupled with a 5 ns pulse Nd:YAG laser (the excitation light source). The output photon energy was 0.85 eV (1.45 μm), which gave an effective photoinduced conversion from the LT to the HT phase via a two-photon absorption for the CT exciton band located at 1.7 eV. The two-photon absorption process can dramatically reduce sample heating, thermal diffusion and stress coming from the spatial excitation inhomogeneity, and therefore, it offers clear information on PIPT.[26,27)] After each one-shot excitation on the LT phase crystal for a given excitation photon density, the THz absorption spectra was measured using broadband THz-TDS.

III. Results and discussion

A. Intermolecular vibrations in the THz frequency region

Figure 2(a) shows the reference THz waveform (inset) and its Fourier transform (FT) on a logarithmic scale. The frequency components ranged widely from 0.1 to 12 THz but could still be detected in our THz-TDS setup. Figures 2(b) and 2(c) show the

FTs of the spectra obtained for the HT and LT phase crystals at RT for $E_{\perp}$ and $E_{//}$ polarizations. Here, $E_{\perp}$ and $E_{//}$ denote the polarizations of the THz electric field perpendicular and parallel to the stacking axis of TTTA molecules, respectively.[23,24] As shown in Figs. 2(b) and 2(c), a strong THz absorption band appeared at 4.0 THz in the $E_{\perp}$ spectra, whilst a weak THz absorption band lay at 1.3 THz in the $E_{//}$ spectra. Note that no THz absorption band was observed in the HT phase for either polarization. Because the observed THz absorption bands lie in the lower THz frequency region, they might be attributed to the intermolecular vibrational modes in the TTTA crystal.

When performing temperature-dependent absorption and precise photolysis measurements, we could not successfully detect the 1.3 THz band probably due to the following reasons. First, the intensity of the 1.3 THz band was ~5 times weaker than that of the 4.0 THz band. Second, the spot size (~300 μm) of the 1.3 THz electric field coming from the diffraction limit is comparable with sizes of the sample width and the sample holder. Because TTTA is highly volatile, the sample width became smaller during the experiments in an air-evacuated cryostat. As a result, some part of the lower THz field might directly pass thorough a gap of the sample holder, and thus, the vibrational peak at 1.3 THz may not be sensitively detected. Therefore, we will now focus on the 4.0 THz band observed in the $E_{\perp}$ spectra.

The FT of the $E_{\perp}$ spectra at different temperatures (on heating and cooling) is shown in Figure 3(a). As the temperature was decreased (cooling), an absorption peak at 4.0 THz suddenly appeared below 230 K. As the temperature was increased (heating), on the other hand, the absorption peak remained up to 310 K where it abruptly decreased. The temperature dependence of this absorption peak on cooling (closed squares) and heating (closed circles) is shown in Fig. 3(b). As a reference, the corresponding ESR signal is also shown by broken and dotted curves for cooling and heating, respectively.[23] As shown in Fig. 3(b), the temperature dependence of the absorption peak at 4.0 THz indicates a first-order phase transition with large hysteresis, and is in quite good agreement with the measured ESR intensity. This indicates that the observed THz absorption peak at 4.0 THz corresponds to an intermolecular vibrational mode that is also relevant to the magnetic phase transition in TTTA.

B. Symmetry arguments of the observed vibrational modes

In order to elucidate the relationship between the observed THz absorption peaks

and the magnetic phase transition, we considered the origin of these modes based on the symmetry of the crystal.[31-33] Focusing on the little group characterized by the wave vector $\boldsymbol{k}=\boldsymbol{0}$ (which is equivalent to the space group itself), we analyzed the intermolecular vibrational modes at the Γ point in the first Brillouin zone. The HT phase has four TTTA molecules per unit cell and belongs to the $P2_1/c$ space group [Fig. 4 (a)],[18,19,33] which has an inversion center, a twofold screw axis, and a glide plane perpendicular to the screw axis. The translation is described by $\boldsymbol{l}=l_a\boldsymbol{t}_a+ l_b\boldsymbol{t}_b+ l_c\boldsymbol{t}_c$ using primitive translation vectors ($|\boldsymbol{t}_a|=a$, $|\boldsymbol{t}_b|=b$, $|\boldsymbol{t}_c|=c$) and the integers, l_a, l_b, l_c. We also define the displacement, $\boldsymbol{r}_n = (x_n, y_n, z_n)$, in the Cartesian coordinate system for each TTTA molecule center (n=1, 2, 3 and 4), as shown in the inset of Fig. 4 (a). The normal intermolecular vibrations at the Γ point are expressed by:

$$\sum_{n=1}^{4}(\alpha_n x_n + \beta_n y_n + \gamma_n z_n)\,, \qquad (1)$$

where the coefficients α_n, β_n, and γ_n indicate the motion of each molecule. Here, the rotational motions of the molecules are ignored because it might not be the dominant contribution to the transition dipole moment. Reduction of the representation matrices obtained by symmetry actions on the displacements results in the classification of the normal vibrational modes of the HT phase. For the HT phase, there are: three A_g modes - linear combinations of x_1-x_2+x_3-x_4, y_1-y_2+y_3-y_4, and z_1+z_2-z_3-z_4; three B_g modes - linear combinations of x_1+x_2-x_3-x_4, y_1+y_2-y_3-y_4, and z_1-z_2+z_3-z_4; two A_u modes - linear combinations of x_1-x_2-x_3+x_4, and y_1-y_2-y_3+y_4; and the B_u mode z_1-z_2-z_3+z_4. In order to confirm whether these vibrational modes are IR active or not, we consider the symmetry properties of an electric moment as well. We found that it should be polarized toward the z (|| b-axis) direction and xy-plane (ac-plane) under A_u and B_u symmetries, respectively. As the vibrational modes of the A_u and B_u symmetries do not match the polarized directions, no IR active mode is expected to appear in the HT phase. Indeed, no IR absorption peaks were observed in the HT phase, as shown in Fig. 2, indicating that the results from symmetry arguments explain the observed experimental results well.

We will now consider the intermolecular vibrations of the LT phase in the same manner. The LT phase also has four molecules per unit cell and belongs to the $P\bar{1}$ space group [Fig. 4(b)],[18, 19, 33] which only has an inversion center with respect to point group actions. As with the HT phase, the normal vibrational modes are classified into:

six A_g modes - linear combinations of $x_1+x_2-x_3-x_4$, $x_1-x_2+x_3-x_4$, $y_1+y_2-y_3-y_4$, $y_1-y_2+y_3-y_4$, $z_1+z_2-z_3-z_4$, and $z_1-z_2+z_3-z_4$; and three A_u modes - linear combinations of $x_1-x_2-x_3+x_4$, $y_1-y_2-y_3+y_4$, and $z_1-z_2-z_3+z_4$. The electric moment in the LT phase is characterized by the A_u representation and will be polarized toward the x, y (|| b-axis), and z directions. As the vibrational modes with A_u symmetry do match suitable polarizations, these A_u modes are IR active and may appear in the LT phase at the THz frequency region. The three optically allowed IR vibrations are shown in Figs. 5(a), 5(b), and 5(c), where the molecular motions of the four TTTA molecules are illustrated by arrows. As shown in Fig. 2, we observed two IR absorption bands in the THz frequency region: the 1.3 THz band for $E_{//}$ spectra and the 4.0 THz band for $E_{\perp}$ spectra. The IR mode vibrating along the stacking direction shown in Fig. 5(c) therefore corresponds to the observed 1.3 THz band. The higher 4.0 THz band in the $E_{\perp}$ spectra originates from the IR vibrational modes illustrated in Figs. 5(a) and 5(b). The single-peaked spectra suggest that these two vibrations may possess almost the same frequency. Since lattice vibrations concerned in phase transitions are normally soft, the lower frequency band might be directly related to the dimerization of TTTA molecules. The observed IR active modes are characteristic of the LT phase, and therefore, the observation of THz absorption bands clearly distinguishes between the LT and HT phases.

C. The photoinduced LT diamagnetic to HT paramagnetic phase transition probed by IR-active intermolecular vibrations

Finally, we shall demonstrate the photoinduced diamagnetic to paramagnetic phase transition of TTTA single crystals probed by broadband THz-TDS. Figure 6(a) shows the FT of the $E_{\perp}$ spectra for the LT (top) and HT (bottom) phases, and intermediate stages obtained by single-shot laser photolysis of the LT phase with different photon densities. In the LT phase, the absorption band relevant to the intermolecular vibration was clearly observed at 4.0 THz. After a single-shot laser pulse with photon densities greater than $3.0\text{x}10^{18}$ photons/cm^2, the absorption intensity decreased and the FT of the $E_{\perp}$ spectrum approached that of the HT phase. Figure 6(b) shows the change in the THz absorption intensity of the 4.0 THz band as a function of excitation photon density. The conversion efficiency from the LT to the HT phase was also estimated from complementary photoinduced Raman measurements and is shown by circles on Fig. 6(b). [27] The THz absorption intensity decreased with increasing

excitation photon density above a threshold photon density of ~3.0×10^{18} photons/cm^2. Note that this threshold value is in good agreement with that of the PL measurement.[27] This indicates that the observed intermolecular vibrations are directly responsible for the PIPT in TTTA.

Under intense photoexcitation, STE states accompanied by local lattice distortions are generated in the LT phase. Subsequently, an excited domain is formed (that multiplies in size) as a precursor for the PIPT. Our present results show that the THz absorption band relevant to the LT phase simultaneously disappears at this stage. Eventually, the PIPT from the LT to the HT phase completes and the Raman modes that characterize the HT phase emerge with slightly higher threshold excitation densities.

IV. Conclusion

In conclusion, we have investigated the intermolecular vibrational modes relevant to the photoinduced magnetic phase transition in strongly correlated organic TTTA crystals using broadband THz-TDS. Two THz absorption bands were observed at 1.3 and 4.0 THz in the LT phase that were not present in the HT phase. The lower frequency absorption band in the LT phase originates from the intermolecular vibration along the dimerization of TTTA molecules, while the higher frequency band comes from the intermolecular vibration perpendicular to the stacking axis. We found that the intermolecular mode at 4.0 THz disappears upon irradiation with an intense light pulse (that exhibited a threshold intensity of 3.0×10^{18} photons/cm^2), indicating a photoinduced phase transition from the LT diamagnetic to the HT paramagnetic phase. These results suggest that the study of intermolecular vibrational modes using broadband THz-TDS is indispensable for revealing the phase transitions.

Acknowledgments

The authors would like to acknowledge T. Takeuchi for his help in the synthesis of the TTTA crystals and Dr. H. Shimosato for his help with the early stage development of the broadband THz-TDS. This work was supported in part by the Grants-in-Aid for Scientific Research (Nos. 23241034, 23104515, 25600113, and 25104712) from the JSPS and MEXT.

References

[1] K. Nasu, *Photoinduced Phase Transitions* (World Scientific Publishing, Singapore, 2004).

[2] K. Yonemitsu and K. Nasu, Phys. Rep. **465**, (2008) 1.

[3] K. Ishida and K. Nasu: Phys. Rev. Lett. **100** (2008) 116403.

[4] S. Koshihara, Y. Tokura, K. Takeda, and T. Koda: Phys. Rev. Lett. **68** (1992) 1148.

[5] O. Sato, T. Iyoda, A. Fujishima, and K. Hashimoto: Science **272** (1996) 704.

[6] Y. Ogawa, S. Koshihara, K. Koshino, T. Ogawa, C. Urano, and H. Takagi: Phys. Rev. Lett. **84** (2000) 3181.

[7] E. Collet, M-H. Lemée-Cailleau, M. Buron-Le Cointe, H. Cailleau, M. Wulff, T. Luty, S. Koshihara, M. Meyer, L. Toupet, P. Rabiller, and S. Techert: Science **300** (2003) 612.

[8] M. Lorenc, J. Hébert, N. Moisan, E. Trzop, M. Servol, M. Buron-Le Cointe, H. Cailleau, M. L. Boillot, E. Pontecorvo, M. Wulff, S. Koshihara, and E. Collet: Phys. Rev. Lett. **103** (2009) 028301.

[9] H. Okamoto, Y. Ishige, S. Tanaka, H. Kishida, S. Iwai, and Y. Tokura: Phys. Rev. B **70** (2004) 165202.

[10] S. Iwai, K. Yamamoto, A. Kashiwazaki, F. Hiramatsu, H. Nakaya, Y. Kawakami, K. Yakushi, H. Okamoto, H. Mori, and Y. Nishio: Phys. Rev. Lett. **98** (2007) 097402.

[11] A. Cavalleri, Cs. Tóth, C. W. Siders, J. A. Squier, F. Ráksi, P. Forget, and J. C. Kieffer, Phys. Rev. Lett. **87** (2001) 237401.

[12] Y. Kawakami, T. Fukatsu, Y. Sakurai, H. Unno, H. Itoh, S. Iwai, T. Sasaki, K. Yamamoto, K. Yakushi, and K. Yonemitsu: Phys. Rev. Lett. **105** (2010) 246402.

[13] K. Onda, S. Ogihara, K. Yonemitsu, N. Maeshima, T. Ishikawa, Y. Okimoto, X. Shao, Y. Nakano, H. Yamochi, G. Saito, and S. Koshihara: Phys. Rev. Lett. **101** (2008) 067403.

[14] J. Hebling, K. -L. Yeh, M. C. Hoffmann, B. Bartal, and K. A. Nelson: J. Opt. Soc. Am. B **25** (2008) B6.

[15] K.W. Kim, A. Pashkin, H. Schäfer, M. Beyer, M. Porer, T. Wolf, C. Bernhard, J. Demsar, R. Huber, and A. Leitenstorfer, Nature Materials **11** (2012) 497.

[16] M. Liu, H. Y. Hwang, H. Tao, A. C. Strikwerda, K. Fan, G. R. Keiser, A. J. Sternbach, K. G. West, S. Kittiwatanakul, J. Lu, S. A. Wolf, F. G. Omenetto, X. Zhang, K. A. Nelson, and R. D. Averitt: Nature **487** (2012) 345.

[17] I. Katayama, H. Aoki, J. Takeda, H. Shimosato, M. Ashida, R. Kinjo, I. Kawayama, M. Tonouchi, M. Nagai, and K. Tanaka: Phys. Rev. Lett. **108** (2012) 097401.

[18] W. Fujita and K. Awaga: Science **286** (1999) 261.

[19] W. Fujita, K. Awaga, H. Matsuzaki, and H. Okamoto: Phys. Rev. B **65** (2002) 064434.

[20] K. Ohno, Y. Noguchi, T. Yokoi, S. Ishii, J. Takeda, and M. Furuya: ChemPhysChem **7** (2006) 1820.

[21] N. Maeshima and K. Yonemitsu: J. Phys. Soc. Jpn. **77** (2008) 074713.

[22] J. Takeda, M. Imae, S. Kurita, and T. Kodaira: Phase Transitions **75** (2002) 863.

[23] J. Takeda, M. Imae, O. Hanado, S. Kurita, M. Furuya, K. Ohno, and T. Kodaira: Chem. Phys. Lett. **378** (2003) 456.

[24] H. Matsuzaki, W. Fujita, K. Awaga, and H. Okamoto: Phys. Rev. Lett. **91** (2003) 017403.

[25] Y. Takahashi, T. Suemoto, S. Oguri, and J. Takeda: Phys. Rev. B **74** (2006) 193104.

[26] T. Kon, S. Oguri, I. Katayama, T. Kodaira, and J. Takeda: Phys. Rev. B **79** (2009) 035106.

[27] I. Katayama, T. Kon, K. Mitarai, and J. Takeda: Phys. Rev. B **80** (2009) 092103.

[28] G. Wolmershäuser and R. Johann: Angew. Chem. Int. Ed. Engl. **28** (1989) 920.

[29] M. Ashida: Jpn. J. Appl. Phys. **47** (2008) 8221.

[30] I. Katayama, H. Shimosato, D. Si. Rana, I. Kawayama, M. Tonouchi, and M. Ashida: Appl. Phys. Lett. **93** (2008) 132903.

[31] E. Bright Wilson, Jr., J. C. Decius, and Paul C. Cross: *Molecular Vibration: The Theory of Infrared and Raman Vibrational Spectra* (McGraw-Hill Book Company, New York, 1955).

[32] A. A. Maradudin and S. H. Vosko: Rev. Mod. Phys. **40** (1968) 1.

[33] J. L. Warren: Rev. Mod. Phys. **40** (1968) 38.

Figure Captions

Figure 1 (color online)
(a) Schematic of the sample holder. Two pieces of thin TTTA crystals with HT phase were mounted onto a copper (Cu) plate. The *b*-axis of the HT phase was aligned (vertically and horizontally) against the side of the sample holder. Two holes not used to mount the samples were made available for measuring polarized reference THz waves. The sample holder was then sandwiched between two thin Cu plates and sealed with Si windows then mounted onto a cold finger. (b) The experimental setup for broadband THz time-domain spectroscopy. To reduce water vapor, the setup was purged by nitrogen gas. Other components of this setup were the HV (high-voltage source); I/V Amp (current amplifier); V/V Amp (voltage amplifier); and PC (personal computer).

Figure 2 (color online)
(a) Fourier transform (FT) of the reference THz waveform on a logarithmic scale; the original THz waveform is shown in the inset. (b) & (c) FT of the THz waveforms for the HT and LT phase crystals at room temperature with $E_{\perp}$ polarization and $E_{//}$ polarization, respectively.

Figure 3 (color online)
(a) Transmitted THz spectra ($E_{\mathrm{TTTA}}/E_{\mathrm{ref}}$) for $E_{\perp}$ polarization at different temperatures whilst cooling and heating. The shaded areas indicate a temperature-dependent absorption band at 4.0 THz. (b) Temperature dependence of the transmittance intensity of the 4.0 THz band upon cooling (solid squares) and heating (solid circles). The temperature dependence of the electron spin resonance (ESR) signals (from Ref. 23) is also shown.

Figure 4 (color online)

(a) Schematic of the HT phase unit cell where a, b, and c indicate the lattice constants. The TTTA molecules highlighted by light (1 and 3) and dark (2 and 4) gray ovals are located at $-b/4$ and $+b/4$, respectively. The tilt of each TTTA molecule is represented by the double-circle and crossed symbols on the carbon atoms whose directions are out of and into the paper, respectively. TTTA molecules are aligned along the b-axis. (b) Schematic of the LT phase unit cell. In the LT phase, TTTA molecules are dimerized perpendicular to the b-axis. The displacements for each TTTA molecule center, $\boldsymbol{r}_n = (x_n, y_n, z_n)$ (where n=1, 2, 3 and 4), in the HT and LT phases are also shown.

Figure 5 (color online)

The three bases of the possible intermolecular IR modes in the LT phase characterized by (a) x_1-x_2-x_3+x_4, (b) y_1-y_2-y_3+y_4, and (c) z_1-z_2-z_3+z_4 vibrations. The molecular motions of the four TTTA molecules in the unit cell are illustrated by arrows.

Figure 6 (color online)

(a) THz transmitted spectra ($E_{\mathrm{TTTA}}/E_{\mathrm{ref}}$) for $E_{\perp}$ polarization after single-shot photolysis with different excitation photon densities. (b) Absorption intensity of the 4.0 THz band and photoinduced Raman intensity (from Ref. 27) as a function of excitation photon density.

Journal of the Physical Society of Japan **83**, 014713 (2014)
http://dx.doi.org/10.7566/JPSJ.83.014713

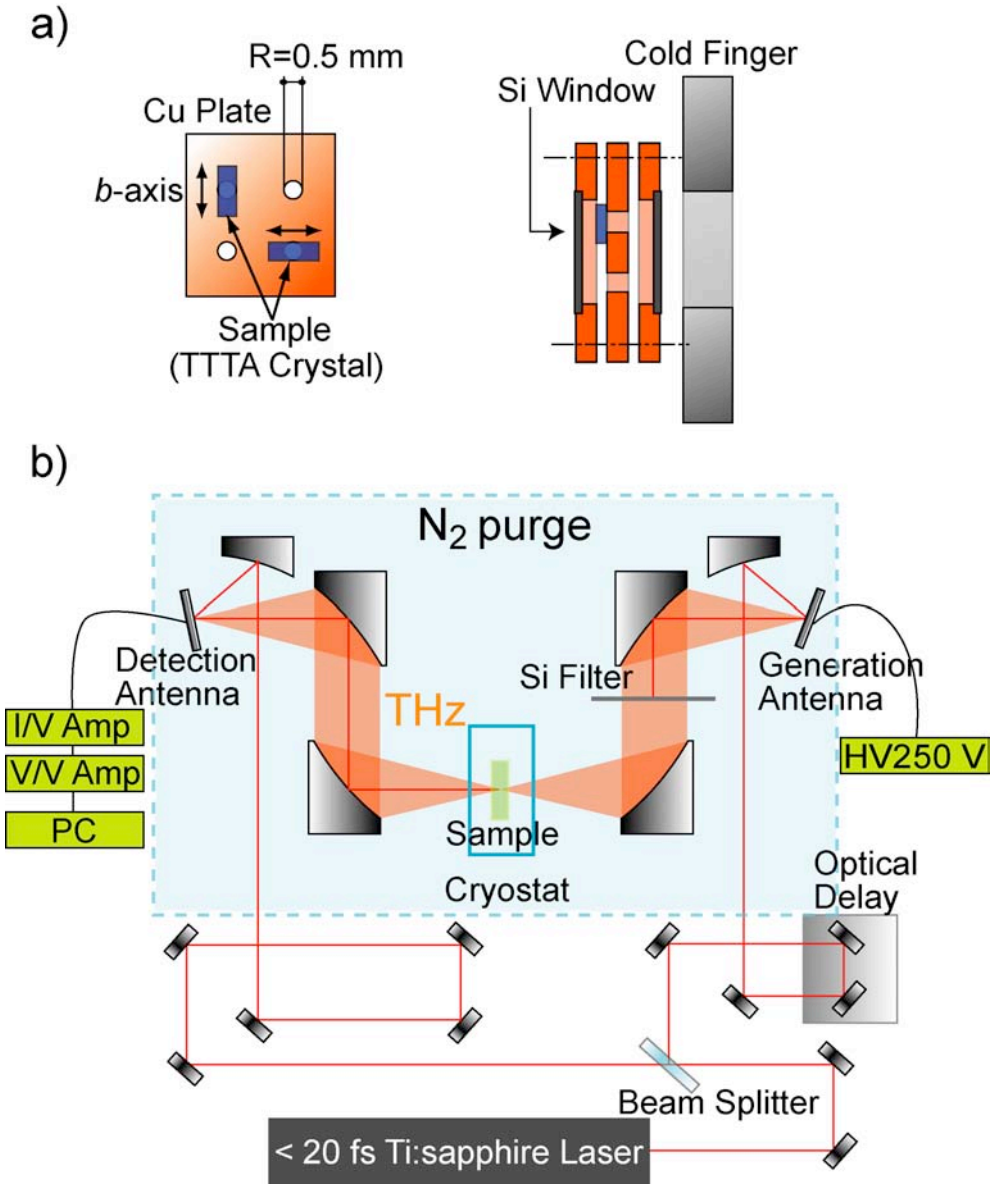

Figure 1

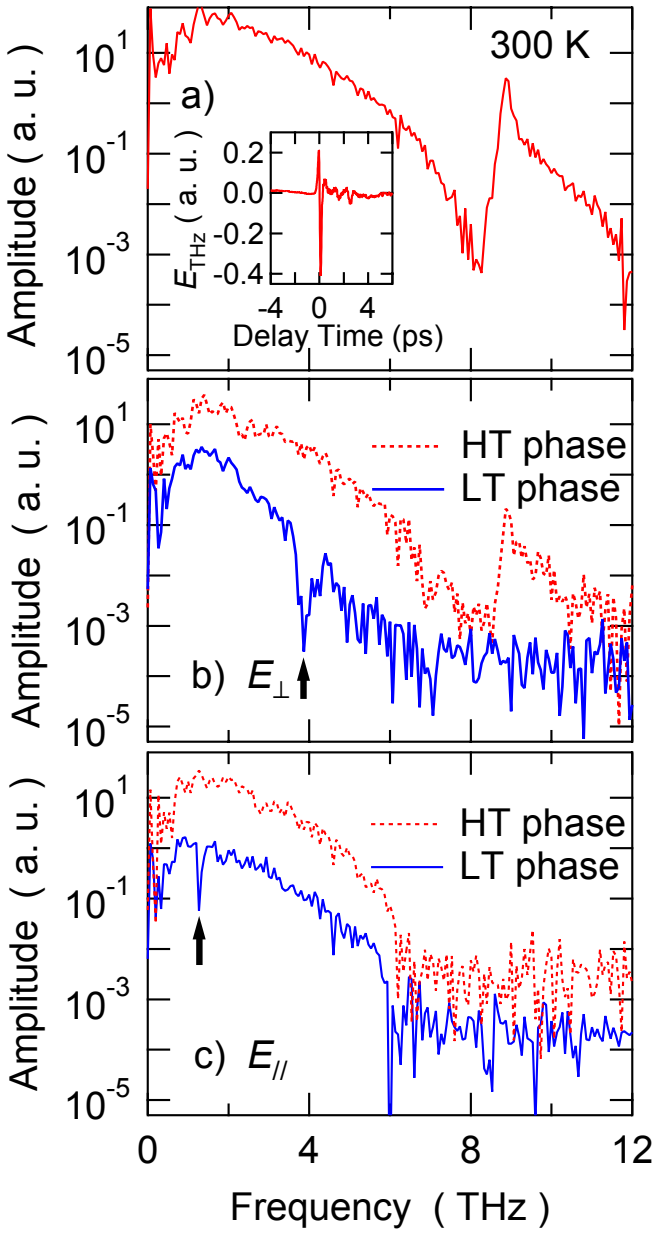
300 K
a)
E_{THz} (a. u.)
0.2
0.0
-0.2
-0.4
-4
0
4
Delay Time (ps)
Amplitude (a. u.)
10^{1}
10^{-1}
10^{-3}
10^{-5}
HT phase
LT phase
b) $E_{\perp}$
c) $E_{//}$
0
4
8
12
Frequency (THz)

Figure 2

Journal of the Physical Society of Japan **83**, 014713 (2014)
http://dx.doi.org/10.7566/JPSJ.83.014713

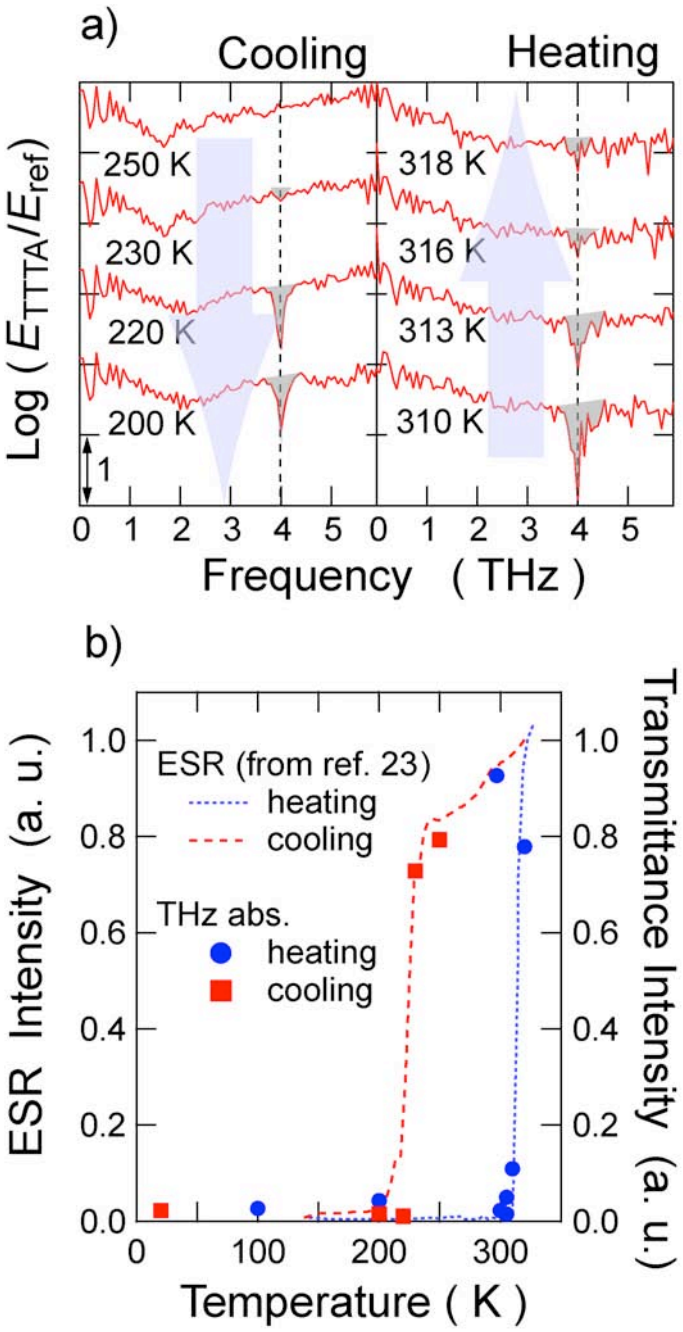

Figure 3

Journal of the Physical Society of Japan **83**, 014713 (2014)
http://dx.doi.org/10.7566/JPSJ.83.014713

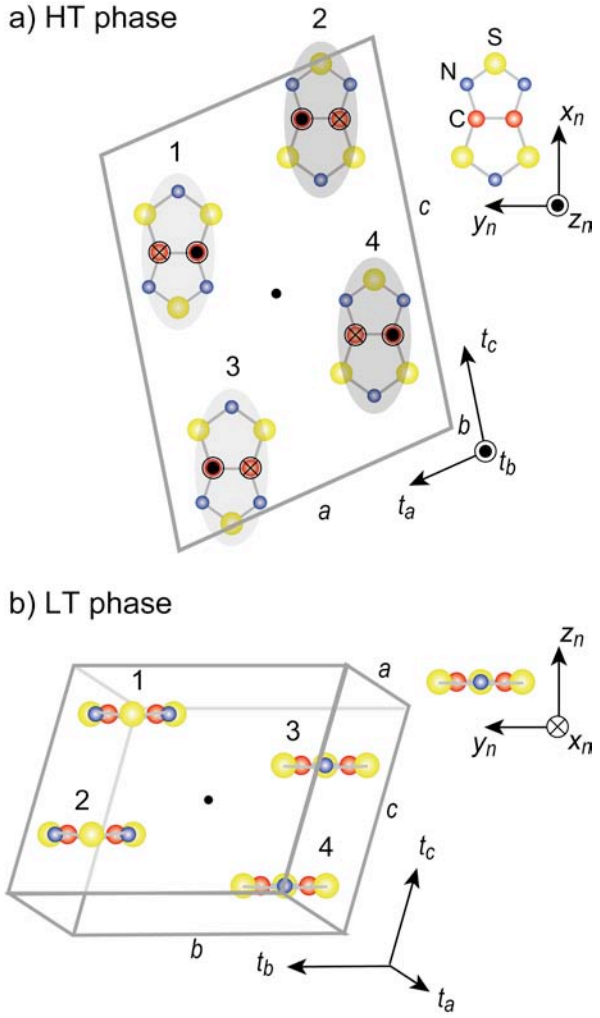

Figure 4

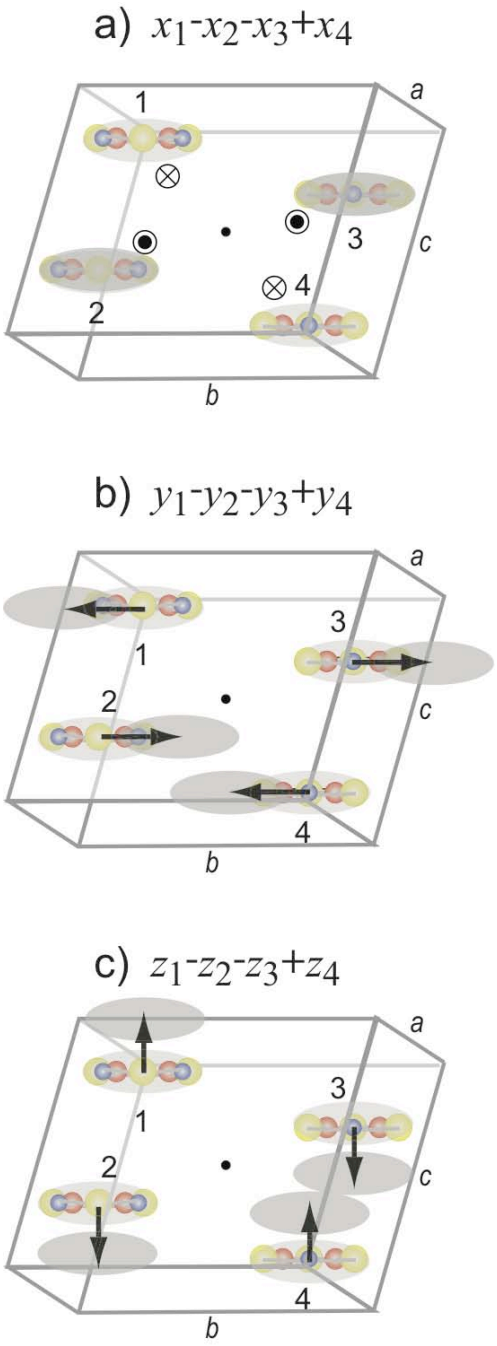

Figure 5

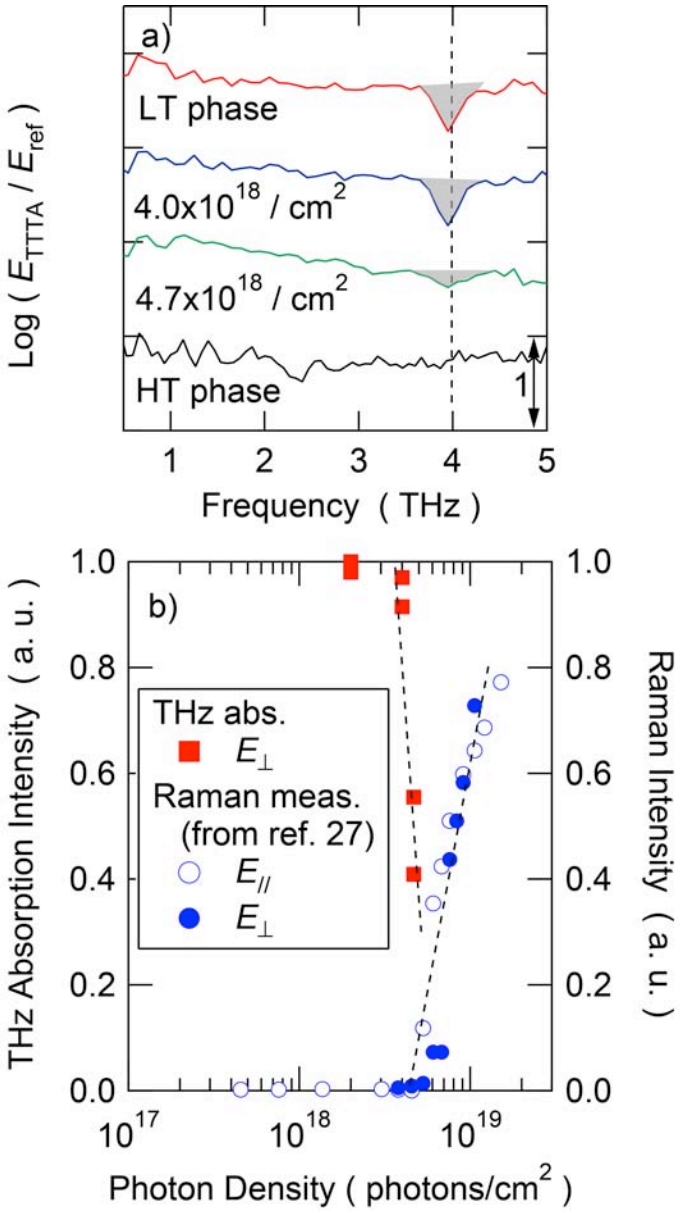
a)
LT phase
4.0x10^18 / cm^2
4.7x10^18 / cm^2
HT phase
1
Log (E_TTTA / E_ref)
Frequency (THz)
b)
THz abs.
E⊥
Raman meas.
(from ref. 27)
E//
E⊥
THz Absorption Intensity (a. u.)
Raman Intensity (a. u.)
Photon Density (photons/cm^2)

Figure 6